THE JOURNAL OF BIOLOGICAL CHEMISTRY VOL. 287, NO. 41, pp. 34764–34775, October 5, 2012

Post-aggregation Oxidation of Mutant Huntingtin Controls the Interactions between Aggregates*[S]

Received for publication, May 30, 2012, and in revised form, July 28, 2012 Published, JBC Papers in Press, August 13, 2012, DOI 10.1074/jbc.M112.387035

Yasushi Mitomi[‡], Takao Nomura[‡], Masaru Kurosawa[§], Nobuyuki Nukina[§], and Yoshiaki Furukawa[‡1]

From the [‡]Laboratory for Mechanistic Chemistry of Biomolecules, Department of Chemistry, Keio University, Yokohama, Kanagawa 223-8522, Japan and the [§]Laboratory for Structural Neuropathology, RIKEN Brain Science Institute, Wako, Saitama 351-0198, Japan

Background: Aggregation of a protein, huntingtin, is a pathological hallmark of Huntington disease.
Results: Oxidation of a methionine in huntingtin occurs only after aggregation and alters the aggregate morphologies.
Conclusion: Properties of protein aggregates can be controlled by a "post-aggregation" modification.
Significance: Learning factors that modulate properties of protein aggregates is relevant to understanding the molecular pathomechanism of neurodegenerative diseases.

Aggregation of protein molecules is a pathological hallmark of many neurodegenerative diseases. Abnormal modifications have often been observed in the aggregated proteins, supporting the aggregation mechanism regulated by post-translational modifications on proteins. Modifications are in general assumed to occur in soluble proteins before aggregation, but actually it remains quite obscure when proteins are modified in the course of the aggregation. Here we focus upon aggregation of huntingtin (HTT), which causes a neurodegenerative disorder, Huntington disease, and we show that oxidation of a methionine residue in HTT occurs *in vitro* and also *in vivo*. Copper ions as well as added hydrogen peroxide are found to oxidize the methionine residue, but notably, this oxidative modification occurs only in the aggregated HTT but not in the soluble state. Furthermore, the methionine oxidation creates additional interactions among HTT aggregates and alters overall morphologies of the aggregates. We thus reveal that protein aggregates can be a target of oxidative modifications and propose that such a "post-aggregation" modification is a relevant factor to regulate properties of protein aggregates.

Misfolding of protein molecules often results in the formation of insoluble aggregates, which are major pathological products observed in many neurodegenerative diseases (1). In proteins composing the aggregates, abnormal post-translational modifications have been often identified, and misregulation of the protein modifications is hence considered to occur under pathogenic conditions and to play roles in the formation of aggregates (2–4).

Post-translational modifications are well known to affect the structural stability of soluble proteins and also the protein-protein interactions (5). Any abnormalities in the modifications hence potentially destabilize the native/functional structure of a protein molecule, which would then facilitate or even trigger the misfolding and aggregation. Abnormally modified proteins are, however, often isolated from insoluble aggregates but not from a soluble fraction of the affected tissues (2, 4), implying that some modifications occur *after* the formation of insoluble aggregates. Given that insoluble aggregates tend to be regarded as final products with inert structures, the protein modifications after aggregation (*i.e.*, "post-aggregation modifications") appear to be underrepresented.

In this study, we have illuminated such post-aggregation modifications by focusing on huntingtin (HTT)[2] as a model protein. HTT is a large protein with approximately 350 kDa of the molecular mass, in which a polyglutamine (polyQ) tract follows the N-terminal 17 amino acids (6). Although a physiological function of HTT is still controversial (7), a normal HTT possesses a polyQ tract with 6–35 consecutive glutamines and localizes at the cytoplasm as a soluble protein (8). In contrast, HTT forms insoluble aggregates in the nucleus as well as the cytoplasm, when the length of a polyQ tract becomes abnormally expanded (>36) (8). Such aggregation of mutant HTT is a pathological hallmark of a neurodegenerative disease, Huntington disease (HD) (9). In the course of HD, oxidative stress has been reported to significantly increase (10); therefore, the aggregates of mutant HTT are supposed to be susceptible to oxidative modifications.

For example, in HD model mice expressing an N-terminal fragment of mutant HTT, abnormal accumulation of copper ions in striatum and cortex, which are the most affected areas of HD, has been observed at a later stage of the disease (11). A copper ion functions as a pro-oxidant and is suggested to oxi-

* This work was supported by Grants-in-Aid 24111542 (to Y. F.) and 22110004 (to N. N.) for Scientific Research on Innovative Areas and Grant-in-Aid 22770162 for Young Scientists (B) (to Y. F.) and Strategic Research Program for Brain Sciences (to N. N.) from the Ministry of Education, Culture, Sports, Science and Technology of Japan, funds from CREST from Japan Science and Technology Agency (to N. N.), a grant-in-aid from the Research Committee for Ataxic Diseases from MHLW (to N. N.), and a grant from the Naito Foundation (to Y. F.).

[S] This article contains supplemental Figs. S1–S6.

[1] To whom correspondence should be addressed: Dept. of Chemistry, Keio University, 3-14-1 Hiyoshi, Kohoku, Yokohama, Kanagawa 223-8522, Japan. Tel.: 81-45-566-1807; Fax: 81-45-566-1697; E-mail: furukawa@chem.keio.ac.jp.

[2] The abbreviations used are: HTT, huntingtin; HD, Huntington disease; HTT^{EX1}, the N-terminal fragment corresponding to the first exon in *HTT* gene; HTT^{N16}, the N-terminal 16 amino acids adjacent to the polyQ tract in HTT; polyQ, polyglutamine; BCS, bathocuproine disulfonate.

dize cysteine residues to form disulfide-linked HTT oligomers (12). Given that almost all of mutant HTT proteins are already aggregated at the disease end stage, however, the aggregation model triggered by oxidative modification on soluble HTT proteins seems questionable. Indeed, at the preclinical stage of the disease, where the inclusions are almost absent, a copper concentration in striatum and cortex is not different between a HD model mouse and its wild-type littermate (11). Recently, furthermore, an aggregation process of mutant HTT has been shown to associate with the production of hydrogen peroxide albeit via an as yet unknown mechanism (13). Compared with soluble HTT proteins, therefore, HTT aggregates are considered to be placed in more oxidative intracellular environments, but it remains unknown whether oxidative modifications occur on HTT aggregates.

We have shown here that Met^8 in HTT is oxidized with copper ions as well as added hydrogen peroxide and found that this Met oxidation occurs only when HTT is in the insoluble aggregated state. A soluble form of HTT is not oxidized even by exogenous addition of copper ions and hydrogen peroxide. We have, furthermore, found that Met oxidation creates additional interactions among HTT aggregates to form the aggregate tangles with increased overall size. We thus propose that a protein remains susceptible for oxidation even in the aggregated state and that properties of protein aggregates can be modulated by such post-aggregation modifications.

EXPERIMENTAL PROCEDURES

Expression and Purification of HTT^{EX1} Proteins—A human HTT^{EX1} cDNA was cloned in an expression vector, pGEX6P-2 (GE Healthcare), using BamHI and XhoI sites; thereby a GST protein was fused at the N terminus of HTT^{EX1} (14). The length of a polyQ tract in human HTT^{EX1} used in this study is either 18 or 42 for an *in vitro* model of normal and mutant HTT, respectively. Furthermore, the six consecutive His residues were directly fused to the C terminus of HTT^{EX1} for facilitation of protein purification. Mutations were introduced by an inverse PCR method using KOD DNA polymerase (TOYOBO), and all constructs used in this study were confirmed by DNA sequencing. *Escherichia coli*, Rosetta(DE3) (Novagen), was transformed with a plasmid, and the expression of HTT^{EX1} proteins was induced with 0.1 mM isopropyl 1-thio-β-D-galactopyranoside at 20 °C at 200 rpm for 48 h.

The cells were lysed with three cycles of freeze and thaw and resuspended in PBS containing 2% Triton X-100, 420 μM $MgCl_2$, and DNaseI. A soluble supernatant was obtained by centrifugation at 14,000 rpm for 10 min, filtrated using a 0.2-μm filter and then mixed with His-SELECT nickel affinity gel (Sigma) (2 ml/40 ml of supernatant). HTT^{EX1} proteins bound on the gel were washed with a buffer at pH 8.0 containing 50 mM Tris, 500 mM NaCl, and 10 mM imidazole and eluted by increasing the concentration of imidazole to 250 mM in the buffer solution. Eluted proteins were further purified by incubating with glutathione-Sepharose high performance (GE Healthcare) on ice for 2 h. After washed with a GST wash buffer (50 mM Tris, 200 mM NaCl, pH 8.0), HTT^{EX1} proteins were collected with a GST elution buffer (50 mM Tris, 200 mM NaCl, 10 mM reduced GSH, pH 8.0). Protein samples were concentrated and ultracentrifuged at 110,000 × *g* for 15 min. The resultant supernatant was subsequently used or stored at −80 °C for further experiments. Concentration of a GST-fused HTT^{EX1} with a His tag was determined from the absorption at 280 nm with an extinction coefficient of 42,860 $cm^{-1}\ M^{-1}$.

Aggregation of Purified HTT^{EX1} Proteins in Vitro—After removal of any insoluble materials by ultracentrifugation, 150 μl of 20 μM GST-HTT^{EX1}-His was prepared in a GST elution buffer. The sample was set in a well of a 96-well plate and mixed with 2 units of a HRV3C protease (Novagen), which specifically cleaves the site between GST and HTT^{EX1}. In this experimental condition, we have confirmed almost completion of the cleavage reactions within 30 min by SDS-PAGE analysis (supplemental Fig. S1). HTT^{EX1}(42Q) liberated from a GST tag has been known to start aggregation, which was monitored by increase in the solution turbidity (the absorbance at 350 nm) using a plate reader (Epoch; BioTek). If necessary, 50 μM bathocuproine disulfonate (BCS), a specific chelator for Cu(I) ions, was added before addition of HRV3C but had no effects on the cleavage reactions by HRV3C protease.

Western Blotting Analysis—After aggregation reactions, 150 μl of samples were fractionated into soluble supernatant and insoluble pellets with ultracentrifugation at 110,000 × *g* for 15 min. Insoluble HTT^{EX1} pellets were washed three times with a buffer containing 50 mM Tris and 200 mM NaCl at pH 8.0 and resolubilized by incubation in 50 μl of TFA at 37 °C for 1 h. TFA was then removed by a centrifugal evaporator (SpeedVac), and the resultant protein pellets were dissolved in 150 μl of a buffer containing 500 mM Tris and 5% SDS at pH 8.0. Soluble supernatant and redissolved pellets were mixed with an SDS-PAGE sample buffer containing 10% β-mercaptoethanol, boiled, and then loaded on a 12.5% SDS-polyacrylamide gel. After electrophoresis, proteins were blotted on a 0.2-μm PVDF membrane and probed with mouse anti-polyglutamine (1C2; Merck Millipore; 1:5000), mouse anti-huntingtin (EM48; Merck Millipore; 1:3000), and mouse anti-GST (WAKO; 1:3000) as primary antibodies. Goat anti-mouse conjugated with HRP (Pierce; 1:3000) was then used as a secondary antibody.

MALDI-TOF Mass Analysis on HTT^{EX1} in Vitro—To analyze a soluble form of HTT^{EX1}, 6 M guanidine HCl and 0.1% TFA were added to the solution, and then the protein was desalted using ZipTip C18 (Millipore). For the mass analysis of HTT^{EX1} protein in the aggregated state, HTT^{EX1} aggregates (40 μg) were first resolubilized with 50 μl of TFA and then dried up by centrifugal evaporator. The protein pellets were then dissolved in 50 μl of 6 M guanidine HCl, acidified by addition of 0.1% TFA, and desalted with ZipTip C18. Sinapic acid was chosen as a matrix, and MALDI-TOF mass spectra were acquired using Ultraflex™ (Bruker) in a reflectron mode. Mass spectra were calibrated using insulin (Nacalai; *m*/*z* 5,734.1), horse heart cytochrome *c* (Nacalai; *m*/*z* 12,361), and equine heart myoglobin (Sigma; *m*/*z* 16,951.5).

To analyze the core regions of HTT^{EX1} aggregates, the aggregates collected by ultracentrifugation were resuspended in a GST elution buffer. After ultrasonication, the aggregates (30 μg, ~40 μl) were mixed with 150 μl of 50 mM Tris, 100 mM NaCl, 5 mM $CaCl_2$, pH 8.0, and then incubated with 5 μg of Pronase at 37 °C for 12 h. Insoluble pellets were collected,

washed twice with a GST wash buffer by ultracentrifugation, and dissolved in 50 μl of TFA with ultrasonication and incubation at 37 °C for 1 h. After removal of TFA with a centrifugal evaporator, the pellets were redissolved in 50 μl of 6 M guanidine HCl with 0.1% TFA, desalted with ZipTip C18, and analyzed with MALDI-TOF mass spectrometry using sinapic acid as a matrix. Mass spectra were further calibrated with insulin (m/z 5,734.1) and horse heart cytochrome *c* (m/z 12,361), and identification of peptides based upon the observed m/z values was performed using PAWS software (ProteoMetrics).

MALDI-TOF Mass Analysis on HTT^{EX1} Aggregates in Vivo—The mouse experiments were approved by the animal experiment committee of the RIKEN Brain Science Institute. A whole brain except cerebellum of an R6/2 mouse (15) at either 8, 12, or 14 weeks of age was homogenized with 3 ml of PBS containing 0.1% Triton X-100, 5 mM EDTA, 0.8 M NaCl, 10% sucrose, and protease inhibitor mixture (Complete-EDTA; Roche Applied Science) using a Teflon homogenizer. After centrifugation at 20,000 × *g*, 4 °C for 20 min, 1% Sarkosyl was added to the supernatant, which was further incubated at room temperature for 2 h. The sample was ultracentrifuged at 110,000 × *g*, 4 °C for 20 min, and the resultant pellets were washed once with 500 μl of PBS containing 5 mM EDTA, 0.8 M NaCl, and 10% sucrose and then once with 500 μl of PBS. The pellets were resuspended with ultrasonication in 100 μl of PBS containing 5 mM EDTA, 0.8 M NaCl, and 50% sucrose and incubated at room temperature for 30 min. After ultracentrifugation at 110,000 × *g* at 4 °C for 20 min, the supernatant was collected, and then the concentration of sucrose was decreased to 10% by adding PBS with 5 mM EDTA and 0.8 M NaCl. Again, the sample was ultracentrifuged; thereby, the pellets were collected as HTT^{EX1} aggregates *in vivo* and resolubilized with the incubation in 100 μl of TFA at 37 °C for 1 h. Successful recovery of HTT^{EX1} was confirmed by Western blotting analysis using an anti-polyglutamine antibody (1C2). Resolubilized HTT^{EX1} aggregates *in vivo* were then dissolved in a buffer (150 μl, pH 8.0) containing 50 mM Tris, 100 mM NaCl, 5 mM $CaCl_2$, and 1 M urea, and further incubated with 2 μg of an endoproteinase Glu-C (Roche Applied Science) at 25 °C for 3 days. After digestion, 80 mg of guanidine HCl and 0.1% (final concentration) of TFA was added, and the supernatant was obtained by ultracentrifugation, desalted with ZipTip C18, and then analyzed by MALDI-TOF mass spectrometry in linear mode using sinapic acid as a matrix. Mass spectra were calibrated by human angiotensin I (Calbiochem; m/z 1,046.2), human ACTH(18–39) (WAKO; m/z 4,930.4), and bombesin (LKT Laboratories; m/z 1619.86).

Electron Microscopy—HTT^{EX1} aggregates were adsorbed on STEM100Cu grids coated by elastic carbon (Okenshoji), washed with water, and then negatively stained with 2% phosphotungstic acid. Images were obtained using an electron microscope (Tecnai^{TM} Spirit, FEI).

Static Laser Light Scattering—HTT^{EX1}(42Q) aggregates prepared in the presence and absence of BCS were analyzed by using SALD-7100H equipped with SALD-71HC (Shimadzu). The data were analyzed by the WingSALD II software (Shimadzu).

Gel Filtration Chromatography—HTT^{N16}(WT and M8A) peptides were chemically synthesized (Biologica) and dissolved in pure water. 100 μl of 10 μM HTT^{N16} peptides were loaded on Nanofilm SEC-150 (Sepax Technologies) fitted to a LaChrom Elite (Hitachi) HPLC system. The column was pre-equilibrated with a buffer containing 50 mM Na-P_i and 100 mM NaCl at pH 7.4, and the flow rate was 0.35 ml/min. The chromatogram was obtained by monitoring the absorbance at 214 nm and calibrated using 100 μl of 0.05 mg/ml human ACTH(18–39) (4,930.4 Da), 0.1 mg/ml human angiotensin I (1,296.5 Da), and 0.05 mg/ml bovine milk α-lactoalbumin (Sigma; 14,200 Da).

RESULTS

Methionine Oxidation in Mutant HTT Occurs after the Formation of Insoluble Aggregates—Full-length HTT is a large protein with ~350 kDa, but the N-terminal fragment corresponding to the first exon in *HTT* gene (HTT^{EX1}) is sufficient for causing HD-like symptoms and neuropathological changes in animal models (15). HTT^{EX1}, which is composed of N-terminal 17 amino acids followed by a polyQ tract and a Pro-rich region, was purified as a fusion protein with GST and then liberated from the GST tag by proteolytic cleavage using a specific protease, HRV3C (16). To evaluate the aggregation kinetics of HTT^{EX1} proteins, we have set 0 min at the time when HRV3C was introduced, although almost (~90%) completion of this proteolytic process required 30 min (supplemental Fig. S1). As shown in Fig. 1*A*, 20 μM HTT^{EX1} with a pathogenic length of a polyQ tract (42Q) increased its solution turbidity, whereas no changes were observed when the length of a polyQ tract is normal (18Q). This reproduces previous findings that aggregation of HTT^{EX1} displays a threshold for polyQ length (17).

Consistent with the nucleation-dependent aggregation model (17), the solution turbidity of HTT^{EX1}(42Q) exhibited a sigmoidal change and reached a plateau at 300 min after the addition of HRV3C, where the aggregation appeared to complete (Fig. 1*A*). Formation of insoluble aggregates was also examined by Western blotting after ultracentrifugal fractionation of the samples into soluble supernatant and insoluble pellets (Fig. 1*B* and supplemental Fig. S2*B*). At 30 min after addition of HRV3C, multiple bands immunoreactive to anti-polyQ antibody (1C2) were observed only in soluble supernatant but not in the pellet fraction (Fig. 1*B*). These bands were also detected with anti-HTT antibody (EM48) but not with anti-GST antibody (supplemental Fig. S2, *A* and *B*). Given that an SDS-PAGE analysis on our starting GST-HTT^{EX1}(42Q) sample has shown a major protein band at 45 kDa with small amounts of impurities (0 min in supplemental Fig. S1), the high molecular weight multiple bands in Fig. 1*B* and supplemental Fig. S2*B* represent the SDS-resistant soluble oligomers of HTT^{EX1}(42Q). Indeed, multiple bands in high molecular weight regions have been previously observed in HTT^{EX1} with an elongated polyQ tract in the electrophoretic analysis (14, 16). Notably, at 300 min after the addition of HRV3C, Western blotting analysis using both 1C2 and EM48 antibodies have shown that all of HTT^{EX1}(42Q) molecules are converted from soluble species into insoluble pellets (Fig. 1*B* and supplemental Fig. S2*B*), supporting the completion of aggregation at 300 min.

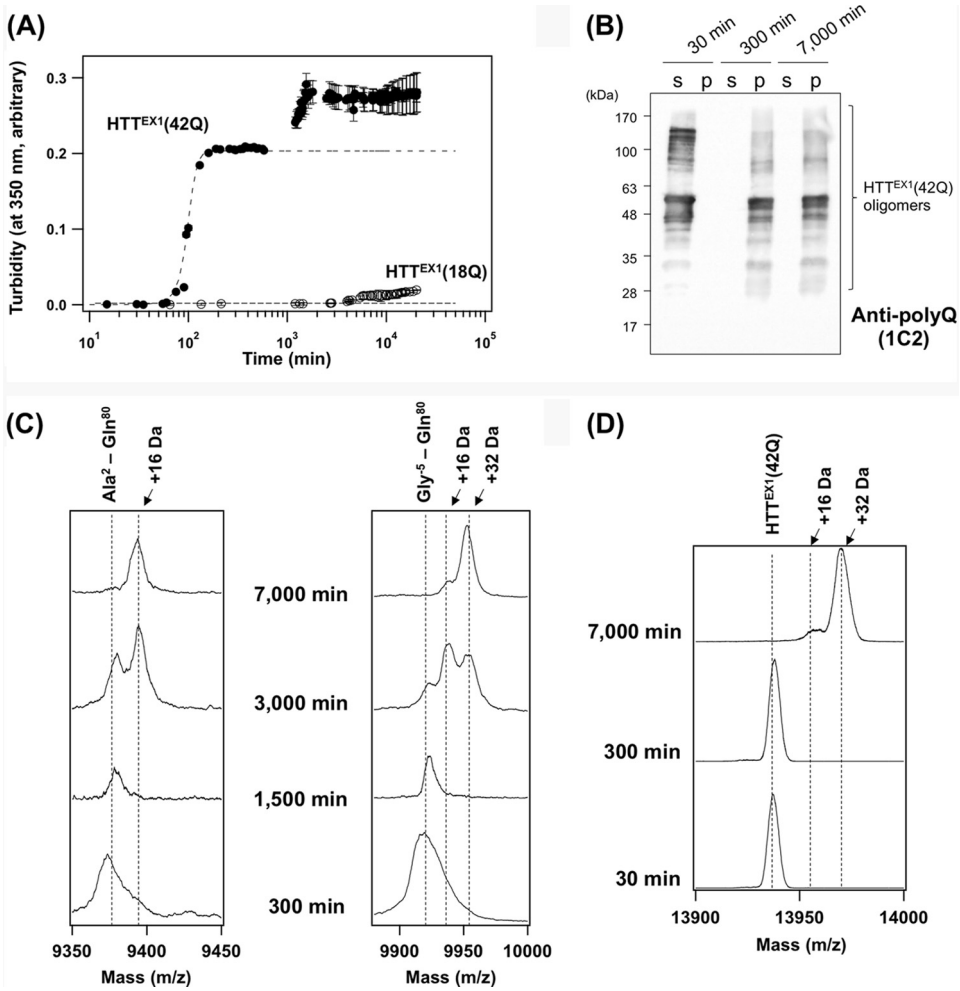

FIGURE 1. **Oxidative modification occurs on HTT^{EX1} after the formation of insoluble aggregates.** *A*, 20 μM GST-fused HTT^{EX1} proteins in a GST elution buffer were incubated at 25 °C with 2 units of HRV3C protease to liberate a HTT^{EX1} fragment, which triggered an aggregation reaction. Increase of the solution turbidity at 350 nm in HTT^{EX1}(42Q) (*filled circles*) until 500 min was fit with a sigmoidal function (*broken curve*). In contrast, HTT^{EX1}(18Q) (*open circles*) did not change its solution turbidity, suggesting no aggregation. *B*, after addition of an HRV3C protease, HTT^{EX1}(42Q) proteins incubated for 30, 300, and 7,000 min were fractionated by ultracentrifugation into soluble supernatant (*s*) and insoluble pellets (*p*). Insoluble pellets were further treated with TFA to resolubilize HTT^{EX1}(42Q) proteins (see "Experimental Procedures"). Both fractions were loaded on a 12.5% SDS-polyacrylamide gel and analyzed by Western blotting with anti-polyQ antibody (1C2). Because of the high aggregation propensity of polyQ-containing proteins, HTT^{EX1}(42Q) proteins were detected as multiple bands in the higher molecular weight region. *C*, pronase-resistant insoluble pellets of HTT^{EX1}(42Q) aggregates at 300, 1,500, 3,000, and 7,000 min were resolubilized with TFA and analyzed by MALDI-TOF mass spectrometry in linear mode. Two representative mass peaks were shown corresponding to Ala^2–Gln^{80} (*left panel*) and Gly^{-5}–Gln^{80} (*right panel*). Other mass peaks were summarized in supplemental Fig. S3. *D*, MALDI-TOF mass analysis (reflectron mode) on the soluble HTT^{EX1}(42Q) before aggregation (30 min) and the insoluble HTT^{EX1}(42Q) aggregates formed at 300 and 7,000 min after incubation. The observed mass of HTT^{EX1}(42Q) coincides with the calculated one (13,937 Da).

Surprisingly, when we further left the solution containing HTT^{EX1}(42Q), the solution turbidity was found to again start to rise (Fig. 1*A*). In our experimental conditions, the time when this second phase of the turbidity increase starts was found to be significantly varied among the sample preparations; however, at 300 min, the first phase of the turbidity increase always finished, and the second phase did not start yet. At 7,000 min, we have consistently confirmed that the second phase of the turbidity increase is almost or completely finished. Furthermore, the second phase of the turbidity change did not simply mean the progression of HTT^{EX1}(42Q) aggregation, because there were no differences in the amounts of pelletable HTT^{EX1}(42Q) between 300 and 7,000 min (Fig. 1*B* and supplemental Fig. S2*B*). We have also confirmed that all HTT^{EX1}(18Q) molecules remain soluble until 7,000 min after the addition of HRV3C (supplemental Fig. S2, *C* and *D*). Given that the solution turbidity depends upon shapes of the scattering particles (or aggregates) (18, 19), we initially suspected that HTT^{EX1}(42Q) aggregates change its molecular structure during the second phase of turbidity changes.

Protein aggregates are generally composed of protease-resistant core and the associated "fuzzy coat" that is a susceptible region for proteolysis (20). To get insight into the structural core of the HTT^{EX1} aggregates before (300 min) and after (7,000 min) the second phase of the turbidity increase, the fuzzy coat regions in the aggregates were removed by treatment with a nonspecific protease, Pronase (21). The resultant Pronase-resistant materials, which were collected as insoluble pellets by ultracentrifugation, were resolubilized with TFA and analyzed by MALDI-TOF mass spectrometry. All of the identified peptides were found to cover a polyQ tract, consistent with its primary role in the formation of aggregates (supplemental Fig. S3). We also

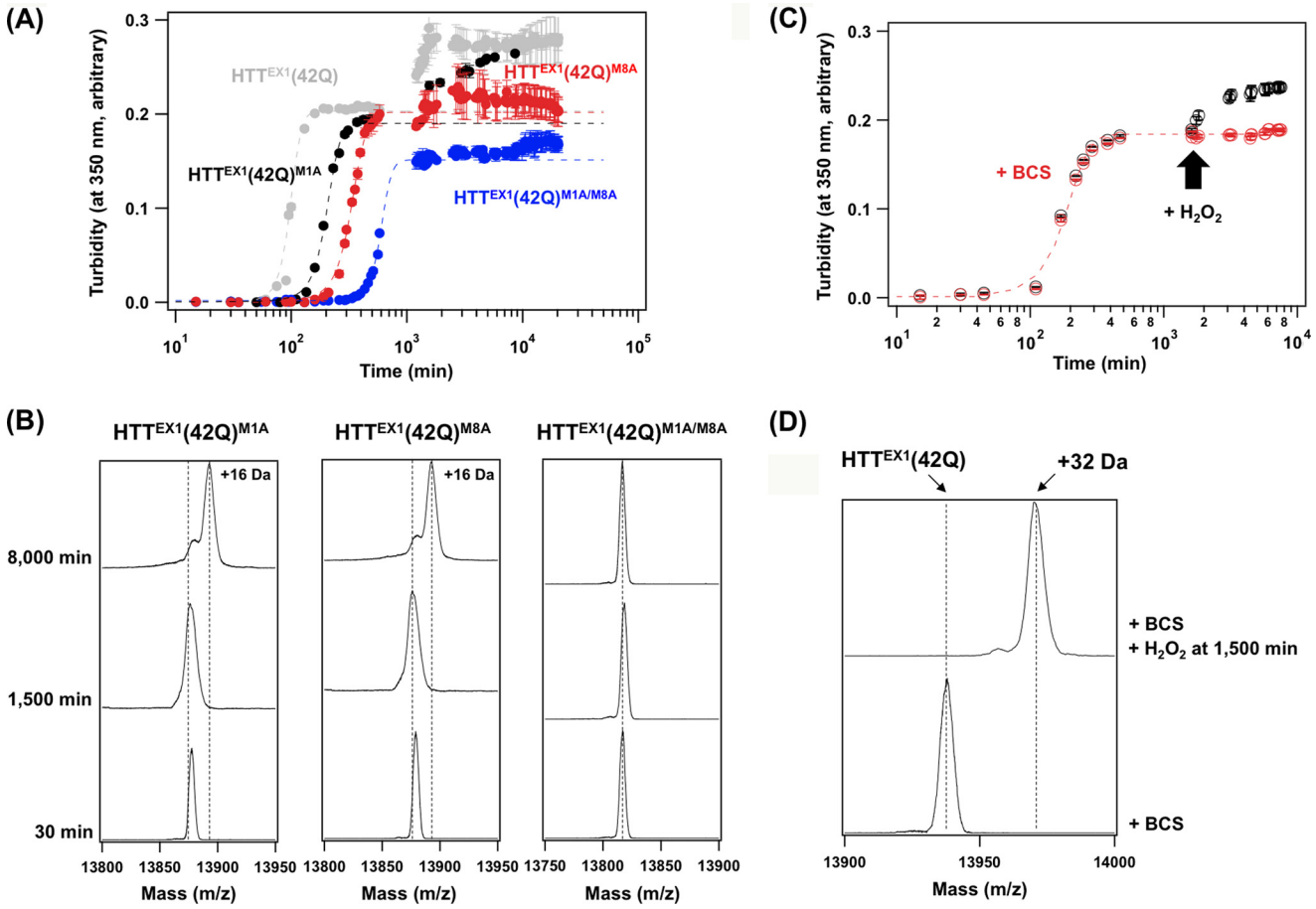

FIGURE 2. **Post-aggregation oxidation at Met^8 in HTT^{EX1}(42Q) causes further increase in solution turbidity.** *A*, aggregation reactions of HTT^{EX1}(42Q) with M1A mutation (*black*), M8A mutation (*red*), and M1A/M8A mutations (*blue*) were examined under the same experimental conditions with those in Fig. 1*A*. For comparison, the aggregation kinetics of HTT^{EX1}(42Q) shown in Fig. 1*A* was also overlaid (*gray*). *Broken curves* represent the sigmoidal fits to the turbidity changes. Note that the second phase of turbidity increase was evident in M1A but not in M8A and M1A/M8A mutant proteins. *B*, MALDI-TOF mass analysis (reflecton mode) on HTT^{EX1}(42Q) proteins with Met mutations was performed before (30 min) and after (1,500 and 8,000 min) aggregation. The observed mass coincides with the calculated one in all samples examined as follows; 13,877 Da (HTT^{EX1}(42Q)^{M1A} and HTT^{EX1}(42Q)^{M8A}) and 13,817 Da (HTT^{EX1}(42Q)$^{M1A/M8A}$). *C*, aggregation kinetics of 20 μM HTT^{EX1}(42Q) in a GST elution buffer in the presence of 50 μM BCS was monitored by the increase of solution turbidity (shown in *red*). Further addition of 0.1 mM H_2O_2 at 1,500 min (indicated with an *arrow*) triggered the second phase of turbidity increase (shown in *black*). *D*, MALDI-TOF mass analysis (reflectron mode) confirms that HTT^{EX1}(42Q) aggregates are not oxidized in the presence of BCS even after 7,000 min incubation (a *lower trace*). In contrast, after H_2O_2 was added at 1,500 min in the presence of BCS (see *C*), the aggregates were collected at 7,000 min and analyzed by MALDI-TOF mass spectrometry (an *upper trace*), showing the 32-Da mass increase.

found that the set of peptides constituting the Pronase-resistant cores of HTT^{EX1}(42Q) aggregates was unchanged during the second phase of the turbidity increase (from 300 to 7,000 min in supplemental Fig. S3). In contrast to our initial expectation, therefore, this result suggests no drastic changes in the core structure of HTT^{EX1}(42Q) aggregates during the post-aggregation process.

Despite this, we have noticed that several Pronase-resistant peptides (No. 8–12 mass peaks in supplemental Fig. S3) exhibit the increase of a 16-Da mass unit during the post-aggregation process. For example, during the second phase of turbidity changes (from 300 to 7,000 min), the mass of the Ala^2–Gln^{80} peptide increased by 16 Da (Fig. 1*C*, *left panel*), and the 16- and 32-Da (16 Da × 2) increases of the mass were observed in the Gly^{-5}–Gln^{80} peptide (Fig. 1*C*, *right panel*). Such increase in the mass was also detected when the analysis was performed on HTT^{EX1}(42Q) (Fig. 1*D*) but not on HTT^{EX1}(18Q) (supplemental Fig. S4). Notably, the 16-Da mass increase was observed in the Met^8–Gln^{80} peptide but not in the Lys^9–Gln^{80} peptide (supplemental Fig. S3); therefore, we suspected that the mass increase of 16 Da represents the oxidation of a Met residue to methionine sulfoxide.

Met^8 in HTT^{EX1} Is Oxidized during the Post-aggregation Increase in the Solution Turbidity—HTT^{EX1} possesses two Met residues at positions 1 and 8, but the initial Met residue has been known to be removed soon after translation *in vivo* (22). Our HTT^{EX1} proteins *in vitro* was, in contrast, prepared by proteolytic cleavage of an N-terminal GST tag, which leaves Met^1 with the tag remnant five amino acids (Gly-Pro-Leu-Gly-Ser) at the N-terminal region (supplemental Fig. S3*B*). We have thus introduced M1A mutation in our *in vitro* HTT^{EX1}(42Q) protein but still observed a second phase of the turbidity change (Fig. 2*A*, *black*) with a 16-Da increase of its mass (Fig. 2*B*, *left panel*). These results are consistent with the idea that the oxidation of Met^8 contributes to a second phase of the turbidity increase. Indeed, M8A mutation in HTT^{EX1}(42Q) abolished the post-aggregation increase of solution turbidity (Fig. 2*A*, *red*), although the mass increase of 16 Da was still observed (Fig.

2*B*, *middle panel*). In HTT^{EX1}(42Q) with M1A/M8A double mutations, neither turbidity increase nor mass increase was observed as the post-aggregation process (Fig. 2, *A*, *blue*, and *B*, *right panel*). It is also notable that a mutation at Met residue significantly delays the aggregation kinetics of HTT^{EX1}(42Q) (Fig. 2*A*). The N-terminal region of HTT^{EX1} has been shown to adopt an amphipathic helix structure, of which the hydrophobic surface plays a role in accelerating the aggregation of HTT^{EX1} with an elongated polyQ tract (23). Met^8 constitutes a hydrophobic surface of the helix (24); therefore, its mutation to Ala will perturb the interactions for aggregation and is thus considered to decelerate the aggregation reaction. In HTT^{EX1}(42Q) with M8A mutation, furthermore, such an increased lag phase (~500 min) before the initial increase of the turbidity might delay the appearance of the second phase; however, we could not observe significant changes in the solution turbidity after 7,000 min at least until 20,000 min (Fig. 2*A*). Based upon these results, therefore, both Met^1 and Met^8 in the aggregated state of HTT^{EX1} *in vitro* are susceptible for oxidation, but only the oxidation of Met^8 leads to the second phase of the turbidity increase.

Oxidation of Met residues is often catalyzed by heavy metal ions (25), and we thus supposed that a trace amount of copper ions often contaminated in chemical reagents and water was responsible for $Met^{1/8}$ oxidation in HTT^{EX1} aggregates. Indeed, when a copper-specific chelator, BCS, was included, the second phase of the turbidity increase completely disappeared in the aggregation of HTT^{EX1}(42Q) (Fig. 2*C*, *red*) without any changes in the mass until 7,000 min (Fig. 2*D*). In contrast, even in the presence of BCS, the addition of an oxidant, H_2O_2, at 1,500 min after incubation started to further increase the solution turbidity (Fig. 2*C*, *black*) and resulted in a mass increase of 32 (16 × 2) Da (Fig. 2*D*). A soluble form of HTT^{EX1}(42Q) before aggregation (at 30 min in Fig. 1*A*) was not oxidized by incubation with 0.1 mM H_2O_2 for 30 min (supplemental Fig. S5*A*). Only when HTT^{EX1}(42Q) aggregates (at 300 min in Fig. 1*A*) were incubated with 0.1 mM H_2O_2 for 30 min was mass increase by 32 Da caused by Met oxidation confirmed (supplemental Fig. S5*B*). Aggregation of HTT^{EX1} would be thus associated with such conformational changes that render Met^8 prone to oxidation. As another negative control, HTT^{EX1}(18Q) was not oxidized by incubating with either copper sulfate or H_2O_2 for 7,000 min (supplemental Fig. S4). Taken together, we have successfully identified the oxidation of Met^8 in HTT^{EX1} that specifically occurs as the post-aggregation process. Our next question is how such a post-aggregation oxidation of Met residues leads to the turbidity increase.

Post-aggregation Control of Interactions between HTT^{EX1} Molecules by Met^8 Oxidation—As mentioned above, factors affecting turbidity include shape, size, and number of particles (aggregates) in solution (18, 19). No changes were confirmed in the amounts of HTT^{EX1} aggregates before and after the oxidation of Met^8 (Fig. 1*B*); furthermore, the protease-resistant core structures of HTT^{EX1} aggregates appeared not to be affected by the oxidation (supplemental Fig. S3). We thus expect that the oxidation of Met^8 somehow increases the overall size of HTT^{EX1} aggregates.

To examine effects of the Met oxidation on the size of HTT^{EX1} aggregates, we first prepared aggregates without and with the oxidation of Met^8 by incubating HTT^{EX1}(42Q) for 7,000 min in the presence and absence of 50 μM BCS, respectively; then these aggregates were directly observed by a transmission electron microscope. Aggregates of HTT^{EX1} with an elongated polyQ tract have been well known to possess fibrillar morphologies (26), which was also confirmed irrespective of the oxidation state at Met^8 in this study (Fig. 3, *A* and *B*). Instead, when the Met residues were oxidized, fibrils were found to more extensively interact with each other, and overall appearance of HTT^{EX1}(42Q) aggregates was changed from the isolated and relatively small tangles (Fig. 3*B*) to the intricate and extended weblike structures (Fig. 3*A*). HTT^{EX1}(42Q) aggregates before oxidation at Met^8 were also examined by incubation for 300 min in the absence of BCS (Fig. 1), and the appearance of those aggregates was confirmed to be similar to the ones prepared by incubation for 7,000 min in the presence of BCS (supplemental Fig. S6*A*). Morphological differences of HTT^{EX1} aggregates before and after oxidation at a Met residue were also observed in HTT^{EX1}(42Q) with M1A mutation (Fig. 3, *C* and *D*); in contrast, the aggregates of HTT^{EX1}(42Q) with M8A mutation remained relatively small and isolated even after incubation for 7,000 min in the absence of BCS (supplemental Fig. S6*B*). These results thus support our idea that the post-aggregation oxidation at Met^8 adds extended interactions between fibrils.

We have further performed quantitative analysis on the size of HTT^{EX1}(42Q) aggregates by static laser light scattering. As shown in Fig. 3 (*E* and *F*), the size of Met-oxidized HTT^{EX1}(42Q) aggregates, which formed at 7,000 min in the absence of BCS, was mainly populated at ~60 μm with a minor fraction of the aggregates smaller than 20 μm (*filled circles*). In contrast, in the HTT^{EX1}(42Q) aggregates formed at 7,000 min in the presence of BCS, where Met^8 remains in the thioether state, significantly more fractions of aggregates exhibited the size smaller than 20 μm (Fig. 3, *E* and *F*, *open circles*). Furthermore, the aggregates formed at 300 min in the absence of BCS, where Met^8 also remains in the thioether state (Fig. 1*A*), were found to be much smaller in size and populated between 0.5 and 5 μm (Fig. 3, *E* and *F*, *open triangles*). Oxidation at Met^8 thus appears not to be an only factor determining the overall size of HTT^{EX1}(42Q) aggregates, but these quantitative results are consistent with our qualitative transmission electron microscope observations on the morphologies of HTT^{EX1}(42Q) aggregates, and the oxidation of Met^8 was confirmed to increase the size of aggregates.

To reveal how the interfibril interactions are augmented by Met oxidation, we focused upon the association state of the N-terminal 16 amino acids (from Ala^2 to Phe^{17}, HTT^{N16}) adjacent to the polyQ tract in HTT. HTT^{N16} was synthesized as a peptide, and its Met^8-oxidized form was prepared by incubation with 100 mM H_2O_2. Successful oxidation was confirmed by MALDI-TOF mass spectrometry; the H_2O_2-treated HTT^{N16} peptide increased its mass by as much as 16 Da (Fig. 4*A*). Besides, these changes were dramatically suppressed in the HTT^{N16} peptide with M8A mutation (Fig. 4*B*), indicating that Met^8 is the most susceptible site for oxidation in HTT^{N16}.

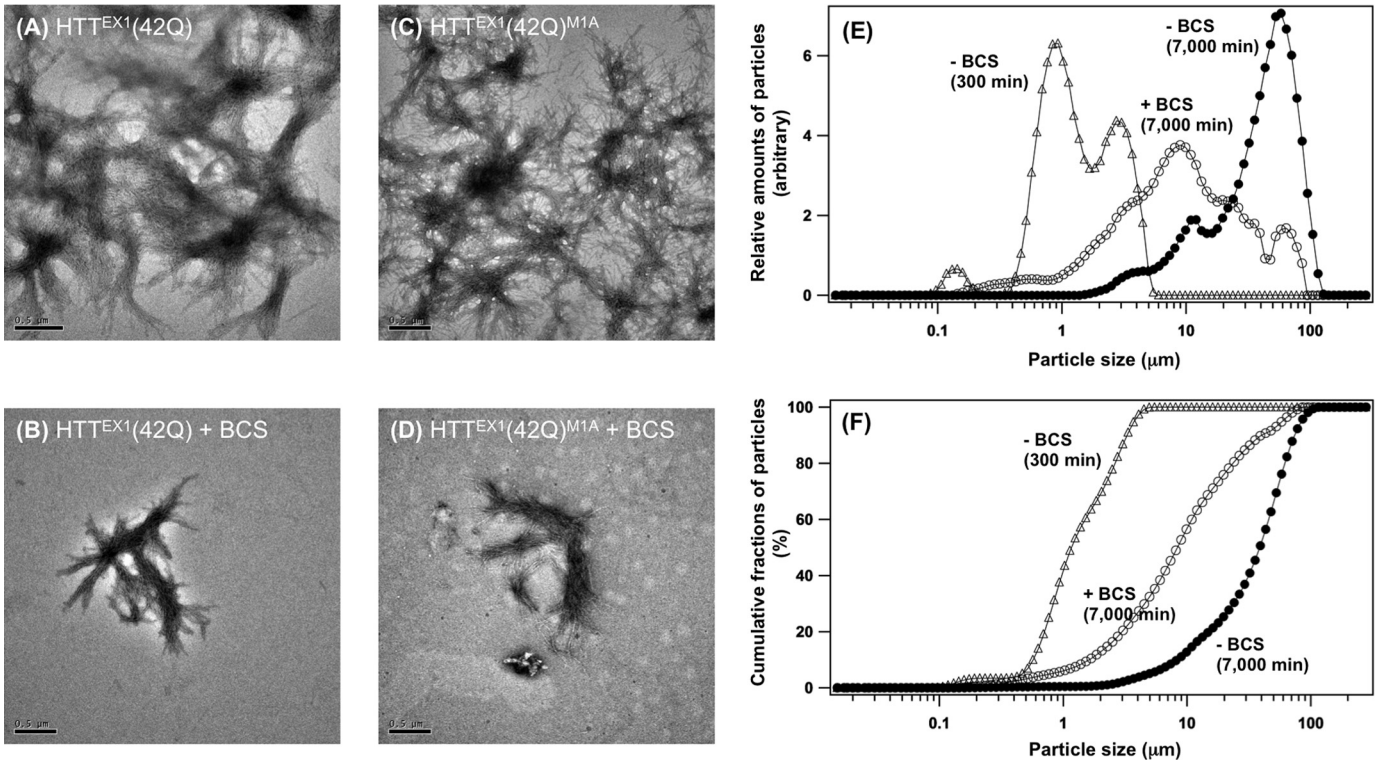

FIGURE 3. **Post-aggregation oxidation at Met^8 facilitates the interactions between HTT^{EX1}(42Q) fibrils to increase overall size of the aggregates.** *A–D*, electron micrograms of HTT^{EX1}(42Q) aggregates (*A* and *B*) and HTT^{EX1}(42Q)^{M1A} (*C* and *D*) aggregates were shown. The aggregates were prepared by incubation of GST-HTT^{EX1}(42Q) proteins with HRV3C in a GST elution buffer for 7,000 min, and 50 μM BCS was further included to inhibit the oxidation of Met residues (*B* and *D*). A *bar* at the *lower left corner* of each panel represents 0.5 μm. *E* and *F*, size of HTT^{EX1}(42Q) aggregates was analyzed by static laser light scattering. Size distribution of HTT^{EX1}(42Q) aggregates, which formed at 7,000 min in the absence (*filled circles*) and presence (*open circles*) of BCS, was shown in *E*. The HTT^{EX1}(42Q) aggregates formed at 300 min after the addition of HRV3C in the absence of BCS were also examined (open triangles). A cumulative distribution of the aggregate size was calculated and plotted in *F*: the aggregates at 7,000 min in the presence (*open circles*) and absence (*filled circles*) of BCS and the aggregates formed at 300 min in the absence of BCS (*open triangles*).

Using these HTT^{N16} peptides, the association states were analyzed by gel filtration chromatography. As shown in Fig. 4*C*, HTT^{N16} was eluted as a single peak corresponding to the monomer size (*open circles*), whereas the oxidation at Met^8 notably associated with the broad peak eluted earlier than the monomer (*filled circles*). HTT^{N16} peptides were thus considered to become easily associated with each other upon the oxidation at Met^8. Although it remains obscure why a slight difference in the retention time of HTT^{N16}(M8A) peptide was observed upon the addition of H_2O_2, a broad peak corresponding to the oligomers of HTT^{N16} was not observed in H_2O_2-treated HTT^{N16} with M8A mutation (Fig. 4*D*). Based upon these results, therefore, the post-aggregation oxidation at Met^8 is considered to promote the interactions between the N-terminal regions of HTT^{EX1}; thereby, the individual fibrils tangle to form the weblike structures, resulting in an increased overall size for aggregates.

Met^8 of HTT Is Oxidized in the Pathological Aggregates of HD Model Mice—Expression of human HTT^{EX1} with an elongated polyQ tract in mice has been known to well reproduce fibrillar aggregation of mutant HTT^{EX1} (15). As performed in the aggregates *in vitro* (Fig. 1*D*), therefore, we attempted to find the 16-Da mass increase of mutant HTT^{EX1} purified from transgenic mice (called R6/2 mice (15)), but it failed to obtain a mass peak corresponding to mutant HTT^{EX1} even after resolubilization with TFA. This is probably because the length of a polyQ tract is relatively long (~130 Q) in mutant HTT^{EX1} expressed in an R6/2 mouse; that is, increasing length of a polyQ tract would make it more difficult to keep HTT^{EX1} soluble and less tolerant for the MALDI-TOF mass analysis. We have thus attempted to perform a mass analysis on soluble fragments that can be produced through a limited proteolysis of mutant HTT^{EX1}.

For that purpose, an endoproteinase, Glu-C, was used for a limited proteolysis of HTT^{EX1}, which can produce a relatively small proteolytic fragment (Lys^6–Glu^{12}) that contains Met^8 but not a polyQ tract. To test whether digestion of HTT^{EX1} with Glu-C produces a Lys^6–Glu^{12} peptide, *in vitro* aggregates of HTT^{EX1}(42Q) before Met^8 oxidation were resolubilized with TFA, incubated with Glu-C and then analyzed with MALDI-TOF mass spectrometry (see "Experimental Procedures"). As shown in Fig. 5 (*trace a*), mass peaks were observed at *m*/*z* 867.95 and 890.50, which correspond to a Lys^6–Glu^{12} peptide and its sodium adduct, respectively. Furthermore, when the Glu-C treatment was performed on *in vitro* aggregates after Met^8 oxidation, a mass peak was observed at *m*/*z* 906.44, which corresponds to a sodium adduct of the Lys^6–Glu^{12} peptide with oxidized Met^8 (Fig. 5, *trace b*). Oxidation of Met^8 in HTT aggregates can thus be examined by mass analysis of the Lys^6–Glu^{12} peptide that is produced by the Glu-C treatment.

Based upon the *in vitro* results above, further *in vivo* testing of the Met^8 oxidation was performed by purification of HTT^{EX1} aggregates from brain tissues of R6/2 mice (see "Experimental

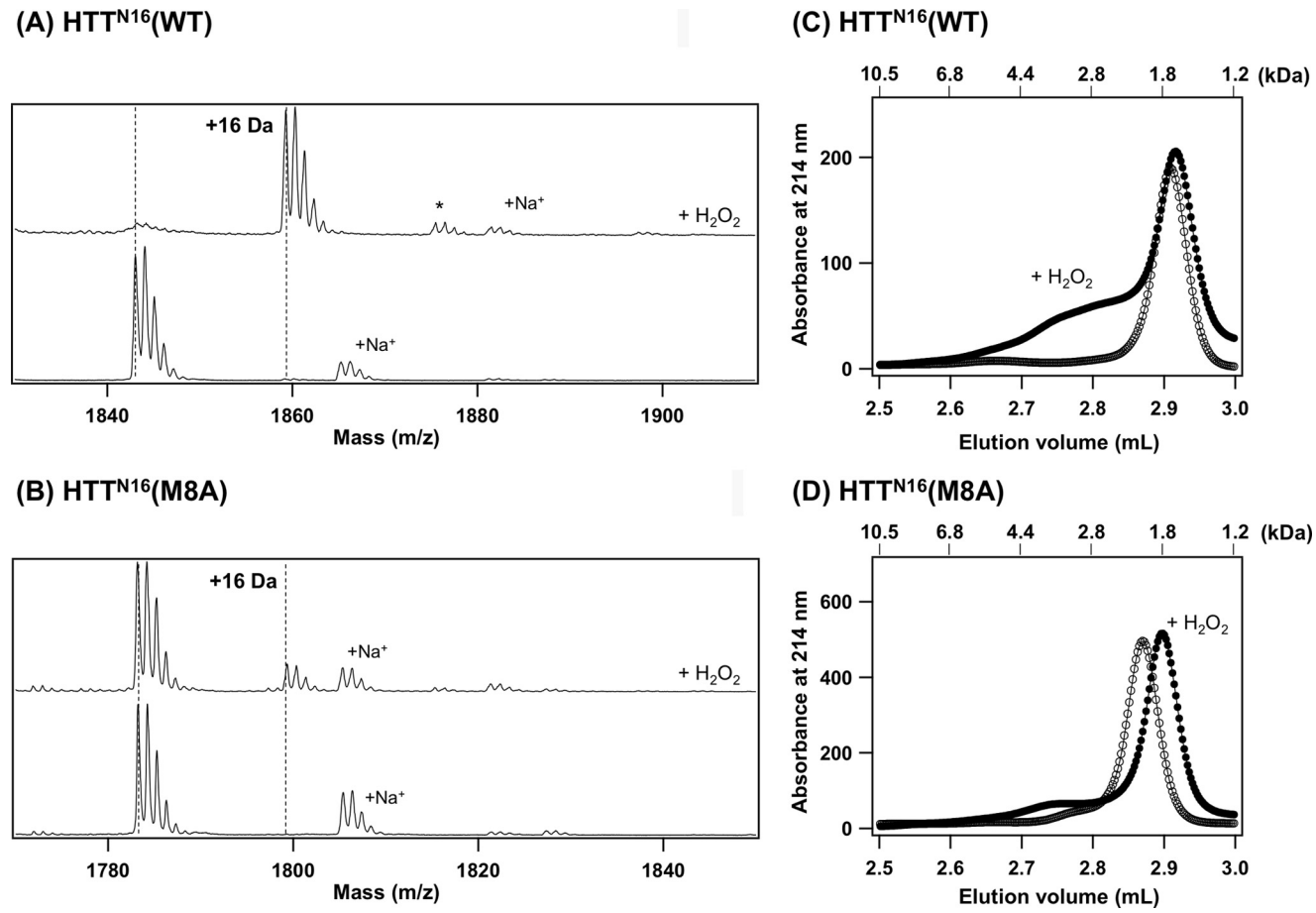

FIGURE 4. **An N-terminal region of HTT^{EX1} (HTT^{N16}) forms oligomers upon oxidation at Met^8.** *A* and *B*, oxidation of HTT^{N16} peptide with hydrogen peroxide was confirmed by MALDI-TOF mass spectrometry in reflectron mode. *A*, HTT^{N16}(WT) (monoisotopic mass, 1842.0) exhibited a mass peak at *m/z* 1843.1, which almost completely shifted to the peak at *m/z* 1859.3 (+16 Da) after treatment with H_2O_2. A minor peak at *m/z* 1875.5 (+32 Da, indicated with an *asterisk*) also appeared, suggesting that the Met oxidation proceeds into the sulfone state in a small fraction of the HTT^{N16} peptide. *B*, in contrast, a mass peak of HTT^{N16}(M8A) (monoisotopic mass, 1782.0) was unchanged at *m/z* 1783.2 even after the addition of H_2O_2, although a minor peak at *m/z* 1799.3 (+16 Da) was observed. Mass peaks indicated with $+Na^+$ are due to the Na^+ adducts of the peptides. *C* and *D*, the gel filtration chromatograms of HTT^{N16}(WT) (*C*) and HTT^{N16}(M8A) (*D*). *Open* and *filled circles* represent the chromatograms of the peptides without and with the addition of H_2O_2, respectively. Molecular mass (kDa) calculated by calibration of the column is also shown on *top* of the figure.

Procedures"). After resolubilized with TFA, the purified *in vivo* aggregates were also treated with Glu-C protease and analyzed by MALDI-TOF mass spectrometry. As shown in Fig. 5 (*traces d*, *f*, and *h*), mass peaks of a Lys^6–Glu^{12} peptide (*m/z* 867) and its sodium adduct (*m/z* 889–890) were observed, and more importantly, we found the mass peak at *m/z* 905–906, which corresponds to the peptide with oxidized Met^8. All of these mass peaks were not observed from insoluble materials isolated from nontransgenic littermates (*traces c*, *e*, and *g*). It is also notable that the mass peak representing the oxidized Met^8 becomes more evident with aging of R6/2 mice. Although MALDI-TOF mass spectrometry is generally not suitable for quantitative analysis, these *in vivo* observations are consistent with our *in vitro* results showing the oxidative modifications on HTT aggregates as a post-aggregation process.

DISCUSSION

Formation of HTT-immunoreactive inclusions in neurons is a pathological hallmark of HD (9). In various rodent models established so far, expression of HTT^{EX1} with an elongated polyQ tract is sufficient for reproduction of the disease pathologies including the formation of inclusions (27). Although the abnormal expansion of polyQ is a primary factor to trigger the aggregation, recent studies have supported modulatory roles of post-translational modifications at the flanking sequence (*i.e.*, the regions other than polyQ in HTT^{EX1}) in the aggregation of mutant HTT. In particular, modifications in HTT^{N16} such as phosphorylation at Ser$^{13/16}$ (28) and sumoylation/ubiquitylation at Lys$^{6/9/15}$ (29) have been shown to affect the aggregation kinetics *in vitro* and *in vivo* and even the HD-like neuropathologies in model animals. Now, as reported here, we add the oxidation at Met^8 as a novel modification in the HTT^{N16} region *in vitro* and *in vivo*, and interestingly, this Met oxidation appears to occur only in the aggregated state of HTT^{EX1} and to regulate the overall morphologies of aggregates (Fig. 6).

In general, Met oxidation is not a rare post-translational modification in proteins; rather, Met belongs to the most easily oxidizable amino acids and forms the sulfoxide even under physiologically mild conditions (30). Notably, the increased oxidative stress has been observed in neurodegenerative diseases including HD (10); therefore, Met residues in proteins are supposed to have an increased chance to be oxidized under

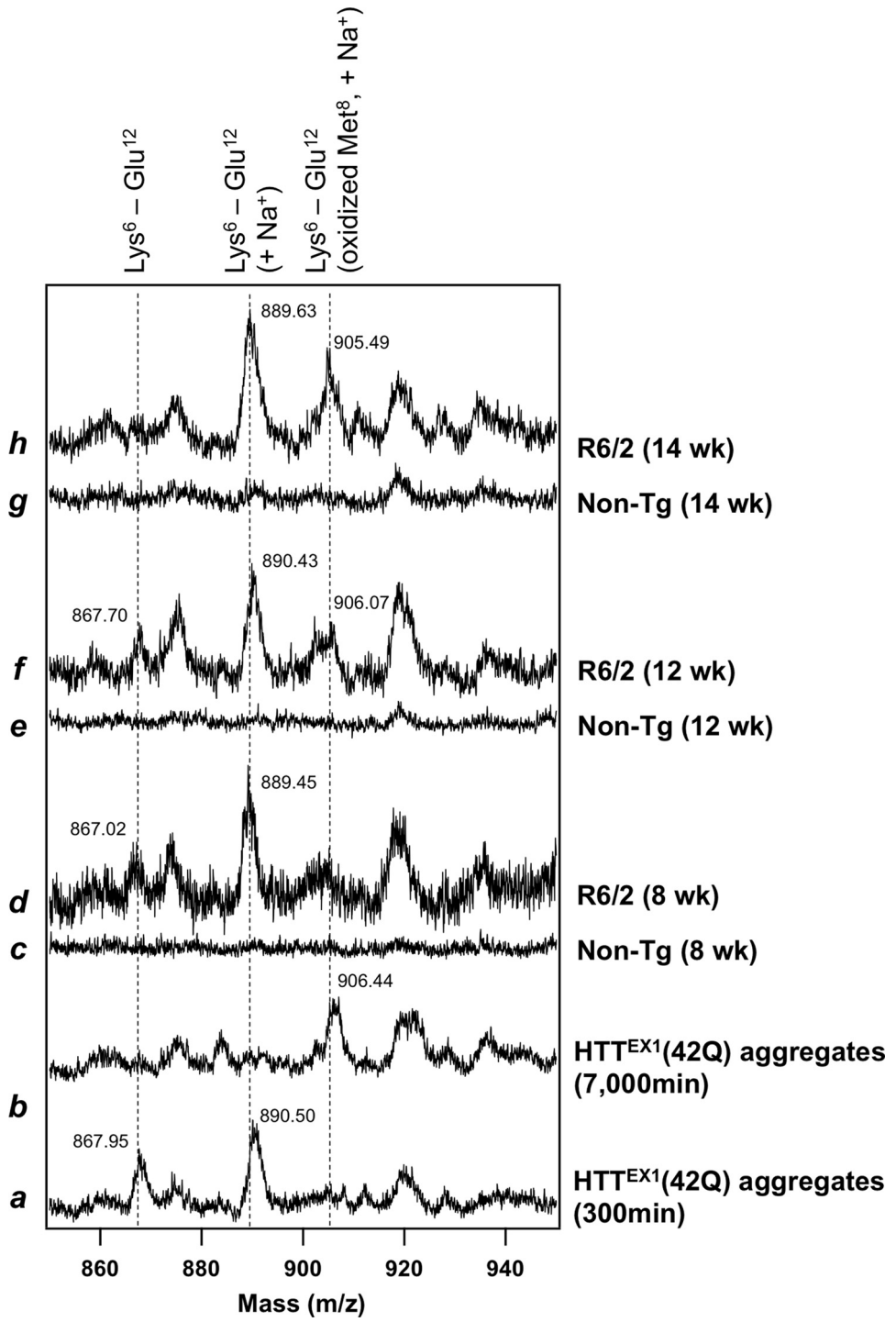

FIGURE 5. **Proteolytic analysis supports the oxidation of Met^{8} in HTT^{EX1} aggregates reproduced in the HD model mouse.** Aggregates of HTT^{EX1}(42Q) *in vitro* (*traces a* and *b*) and HTT^{EX1} purified from R6/2 mice (*traces d*, *f*, and *h*; 8, 12, and 14 weeks of age; see on the *right* of figure) were first redissolved in TFA and treated with Glu-C protease. The resultant proteolytic fragments were then analyzed with MALDI-TOF mass spectrometry in linear mode. A Lys^{6}-Glu^{12} peptide (calculated *m/z* 866.09) exhibited a mass peak at *m/z* 866–867, and the mass peak of its sodium adduct (+23 Da) was also observed at *m/z* 889–890. Furthermore, the mass peak observed at *m/z* 905–906 represents a sodium adduct of a Lys^{6}–Glu^{12} peptide with oxidized Met^{8}. The observed *m/z* values were also shown at mass peaks in the figure. These mass peaks were not obtained when nontransgenic mice were analyzed instead of R6/2 mice (*traces c*, *e*, and *g*), supporting that the mass peaks were assigned to the proteolytic fragments of HTT^{EX1}.

pathogenic/pathological environment. Indeed, for example, oxidation of a Met residue has been reported in an Aβ peptide forming senile plaques of Alzheimer's diseases (31) and also in infectious forms of PrP proteins in prion diseases (32). Furthermore, the effects of Met oxidation on the kinetics of fibrillar aggregation *in vitro* have been examined in several disease-related proteins such as α-synuclein (33), PrP (34), and ApoA-I (35). In these previous studies, oxidative modifications have been assumed to precede the aggregation of protein molecules and thereby affect its formation kinetics; however, it remains obscure when proteins are oxidized during the formation of pathological inclusions *in vivo*. Given that aggregates generally

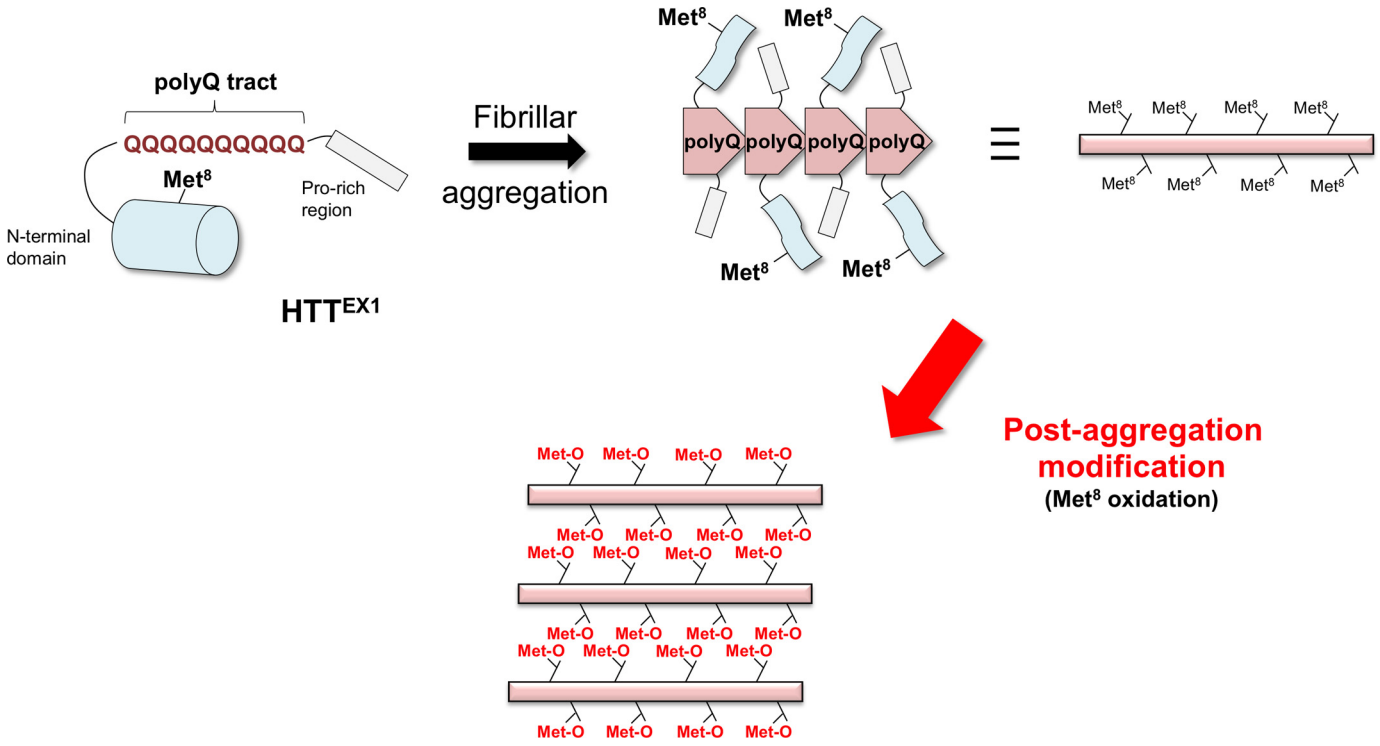

FIGURE 6. **Schematic representation of our proposed mechanism on a post-aggregation modification in mutant HTT proteins.** HTT^{EX1} is composed of an N-terminal region followed by a polyQ tract and a Pro-rich region. In a soluble state shown on the *upper left*, an N-terminal region of HTT^{EX1} has been proposed to adopt an α-helical structure, which is represented as a *cylinder*. When a polyQ tract is abnormally expanded, HTT^{EX1} forms fibrillar aggregates, in which the elongated polyQ constitutes a structural core (shown on the *upper right*). Upon fibrillar aggregation, the N-terminal region would be structurally disturbed, which is further supposed to render Met^8 susceptible for oxidation. Oxidation at Met^8 then introduces the interactions between fibrils via N-terminal regions of HTT^{EX1}, resulting in a size increase for HTT^{EX1} aggregates.

adopt tightly packed structures (36), small oxidants could not attack the amino acid residues in the core but are expected to be accessible to the residues in solvent-exposed regions of aggregates. It is hence possible that some of the protein oxidations occur at the solvent-exposed surface of pathological inclusions even *after* aggregation. Indeed, we have found here that Met^8 is not a constituent of the protease-resistant core in HTT^{EX1} aggregates and is susceptible to post-aggregation oxidation (Fig. 6).

In soluble HTT^{EX1} with nonpathogenic length of a polyQ tract, HTT^{N16} region adopts an amphipathic α-helical structure (37), where Met^8 occupies the central area of the nonpolar surface. Met^8 is thus supposed to be buried in hydrophobic cores formed by HTT^{EX1} proteins (23) and protected from the attack by oxidants such as hydrogen peroxide; indeed, computer simulations have supported the compact conformation of a HTT fragment comprising HTT^{N16} and a polyQ tract (38), where hydrophobic residues in HTT^{N16} are sequestered in the interface between HTT^{N16} and a polyQ tract. In contrast, Met^8 became oxidized in the aggregated state of HTT^{EX1} (Figs. 1 and 2), implying conformational changes of HTT^{N16} upon aggregation. In several studies, HTT^{N16} has been proposed to be incorporated into the core structures of fibrillar HTT^{EX1} aggregates (23, 39), but we have found that a polyQ tract but not the HTT^{N16} region constitutes a protease-resistant core in the aggregates (supplemental Fig. S3). Notably, our results are consistent with recent solid state NMR studies showing that HTT^{N16} region remains α-helical even in the aggregates but display increased dynamics and water exposure (40). As summarized in Fig. 6, therefore, the hydrophobic surface of α-helical HTT^{N16} is covered by a polyQ tract in the soluble state, but upon aggregation, polyQ undergoes significant structural changes to constitute a core of fibrils, which would abrogate the interaction between HTT^{N16} and a polyQ tract. These structural changes associated with aggregation are then considered to increase the exposure of hydrophobic surface of HTT^{N16} and facilitate the oxidation of Met^8.

In our *in vitro* experiments, Met oxidation appears to create new interactions between HTT^{EX1} fibrils and thus increases the overall size of aggregates (Fig. 3). Although a molecular mechanism describing the oxidation-dependent increase in size of aggregates remains to be established, a Met residue has been known to become less hydrophobic or even hydrophilic upon its oxidation from thioether into sulfoxide form (41). Such drastic changes in chemical properties of Met would contribute to the oxidation-induced formation of oligomeric structures in a HTT^{N16} peptide (Fig. 4). As schematically shown in Fig. 6, we thus speculate that the HTT^{N16} region behaves like an oxidation-induced "zipper" to connect the individual HTT^{EX1} fibrils, increasing the overall size of aggregates.

Understanding roles of our proposing post-aggregation oxidation in the disease pathomechanism will require further investigations. Although both toxic and beneficial roles of protein aggregation in the pathomechanism of HD have been suggested (15, 42), distinct conformations of HTT^{EX1} fibrils have been found to exhibit different cytotoxicity toward cultured neuronal cells (43). Although the relation between fibril conformations and toxicity still remains unclear, it is possible that the

potential cytotoxicity of HTT aggregates is modulated through those morphological changes upon the Met oxidation. Interestingly, an age-dependent increase in the size of the cytoplasmic HTT aggregates has been observed in biochemical as well as histological examinations on R6/2 HD model mice (44, 45), in which we have confirmed that pathological HTT^{EX1} proteins are oxidized at its Met^8 residue (Fig. 5). Furthermore, the neuropil aggregates in the HD patients have been reported to increase in size as the disease progresses (46). Nonetheless, the age-dependent increase in the aggregate size can also be interpreted as the simple accumulation of mutant HTT in surviving neurons; therefore, further investigation is also required to reveal pathological roles of Met oxidation as a zipper to increase the size of aggregates in HD.

In conclusion, we propose a mechanism describing the post-aggregation modification on protein aggregates, where structural changes caused by aggregation play critical roles. Significant changes in structures upon aggregation have not been limited to HTT but so far suggested in many other pathogenic proteins (21, 47–49). Post-aggregation modifications are thus supposed to describe pathological changes such as oxidation and phosphorylation detected in inclusions. Although exact roles of post-aggregation modifications in disease pathomechanisms remain to be established, insoluble aggregates are not considered to be inert products of protein misfolding but are able to change its morphologies and structures by post-aggregation modifications. Increasing evidence has recently supported the idea that different structures/morphologies of protein aggregates are related to distinct phenotypes (43, 50, 51); therefore, a possible outcome of post-aggregation modifications may be to modulate disease phenotypes/symptoms even after the onset of disease.

Acknowledgments—We thank Prof. Shuji Akiyama (Institute for Molecular Science, Okazaki, Japan) for fruitful discussion on light scattering and Drs. Mitsuru Maruyama and Atsushi Masumoto (Shimadzu, Japan) for the particle analysis using static laser light scattering.

REFERENCES

1. Ross, C. A., and Poirier, M. A. (2004) Protein aggregation and neurodegenerative disease. *Nat. Med.* **10,** (Suppl.) S10–S17
2. Furukawa, Y., Fu, R., Deng, H. X., Siddique, T., and O'Halloran, T. V. (2006) Disulfide cross-linked protein represents a significant fraction of ALS-associated Cu,Zn-superoxide dismutase aggregates in spinal cords of model mice. *Proc. Natl. Acad. Sci. U.S.A.* **103,** 7148–7153
3. Grundke-Iqbal, I., Iqbal, K., Tung, Y. C., Quinlan, M., Wisniewski, H. M., and Binder, L. I. (1986) Abnormal phosphorylation of the microtubule-associated protein Tau (tau) in Alzheimer cytoskeletal pathology. *Proc. Natl. Acad. Sci. U.S.A.* **83,** 4913–4917
4. Neumann, M., Sampathu, D. M., Kwong, L. K., Truax, A. C., Micsenyi, M. C., Chou, T. T., Bruce, J., Schuck, T., Grossman, M., Clark, C. M., McCluskey, L. F., Miller, B. L., Masliah, E., Mackenzie, I. R., Feldman, H., Feiden, W., Kretzschmar, H. A., Trojanowski, J. Q., and Lee, V. M. (2006) Ubiquitinated TDP-43 in frontotemporal lobar degeneration and amyotrophic lateral sclerosis. *Science* **314,** 130–133
5. Seet, B. T., Dikic, I., Zhou, M. M., and Pawson, T. (2006) Reading protein modifications with interaction domains. *Nat. Rev. Mol. Cell Biol.* **7,** 473–483
6. Huntington's Disease Collaborative Research Group (1993) A novel gene containing a trinucleotide repeat that is expanded and unstable on Huntington's disease chromosomes. The Huntington's Disease Collaborative Research Group. *Cell* **72,** 971–983
7. Cattaneo, E., Zuccato, C., and Tartari, M. (2005) Normal huntingtin function. An alternative approach to Huntington's disease. *Nat. Rev. Neurosci.* **6,** 919–930
8. DiFiglia, M., Sapp, E., Chase, K., Schwarz, C., Meloni, A., Young, C., Martin, E., Vonsattel, J. P., Carraway, R., and Reeves, S. A. (1995) Huntingtin is a cytoplasmic protein associated with vesicles in human and rat brain neurons. *Neuron* **14,** 1075–1081
9. Zoghbi, H. Y., and Orr, H. T. (2000) Glutamine repeats and neurodegeneration. *Annu. Rev. Neurosci.* **23,** 217–247
10. Browne, S. E., Bowling, A. C., MacGarvey, U., Baik, M. J., Berger, S. C., Muqit, M. M., Bird, E. D., and Beal, M. F. (1997) Oxidative damage and metabolic dysfunction in Huntington's disease. Selective vulnerability of the basal ganglia. *Ann. Neurol.* **41,** 646–653
11. Fox, J. H., Kama, J. A., Lieberman, G., Chopra, R., Dorsey, K., Chopra, V., Volitakis, I., Cherny, R. A., Bush, A. I., and Hersch, S. (2007) Mechanisms of copper ion mediated Huntington's disease progression. *PLoS One* **2,** e334
12. Fox, J. H., Connor, T., Stiles, M., Kama, J., Lu, Z., Dorsey, K., Liebermann, G., Sapp, E., Cherny, R. A., Banks, M., Volitakis, I., DiFiglia, M., Berezovska, O., Bush, A. I., and Hersch, S. M. (2011) Cysteine oxidation within N-terminal mutant huntingtin promotes oligomerization and delays clearance of soluble protein. *J. Biol. Chem.* **286,** 18320–18330
13. Hands, S., Sajjad, M. U., Newton, M. J., and Wyttenbach, A. (2011) *In vitro* and *in vivo* aggregation of a fragment of huntingtin protein directly causes free radical production. *J. Biol. Chem.* **286,** 44512–44520
14. Furukawa, Y., Kaneko, K., Matsumoto, G., Kurosawa, M., and Nukina, N. (2009) Cross-seeding fibrillation of Q/N-rich proteins offers new pathomechanism of polyglutamine diseases. *J. Neurosci.* **29,** 5153–5162
15. Davies, S. W., Turmaine, M., Cozens, B. A., DiFiglia, M., Sharp, A. H., Ross, C. A., Scherzinger, E., Wanker, E. E., Mangiarini, L., and Bates, G. P. (1997) Formation of neuronal intranuclear inclusions underlies the neurological dysfunction in mice transgenic for the HD mutation. *Cell* **90,** 537–548
16. Scherzinger, E., Lurz, R., Turmaine, M., Mangiarini, L., Hollenbach, B., Hasenbank, R., Bates, G. P., Davies, S. W., Lehrach, H., and Wanker, E. E. (1997) Huntingtin-encoded polyglutamine expansions form amyloid-like protein aggregates in vitro and in vivo. *Cell* **90,** 549–558
17. Wetzel, R. (2012) Physical chemistry of polyglutamine. Intriguing tales of a monotonous sequence. *J. Mol. Biol.* 421, 466–490
18. Meyer, R. A., and Brunsting, A. (1975) Light scattering from nucleated biological cells. *Biophys. J.* **15,** 191–203
19. Akiyama, S. (2010) Quality control of protein standards for molecular mass determinations by small-angle X-ray scattering. *J. Appl. Crystallogr.* **43,** 237–243
20. Wischik, C. M., Novak, M., Thøgersen, H. C., Edwards, P. C., Runswick, M. J., Jakes, R., Walker, J. E., Milstein, C., Roth, M., and Klug, A. (1988) Isolation of a fragment of tau derived from the core of the paired helical filament of Alzheimer disease. *Proc. Natl. Acad. Sci. U.S.A.* **85,** 4506–4510
21. Furukawa, Y., Kaneko, K., Yamanaka, K., and Nukina, N. (2010) Mutation-dependent polymorphism of Cu,Zn-superoxide dismutase aggregates in the familial form of amyotrophic lateral sclerosis. *J. Biol. Chem.* **285,** 22221–22231
22. Aiken, C. T., Steffan, J. S., Guerrero, C. M., Khashwji, H., Lukacsovich, T., Simmons, D., Purcell, J. M., Menhaji, K., Zhu, Y. Z., Green, K., Laferla, F., Huang, L., Thompson, L. M., and Marsh, J. L. (2009) Phosphorylation of threonine 3. Implications for Huntingtin aggregation and neurotoxicity. *J. Biol. Chem.* **284,** 29427–29436
23. Tam, S., Spiess, C., Auyeung, W., Joachimiak, L., Chen, B., Poirier, M. A., and Frydman, J. (2009) The chaperonin TRiC blocks a huntingtin sequence element that promotes the conformational switch to aggregation. *Nat. Struct. Mol. Biol.* **16,** 1279–1285
24. Thakur, A. K., Jayaraman, M., Mishra, R., Thakur, M., Chellgren, V. M., Byeon, I. J., Anjum, D. H., Kodali, R., Creamer, T. P., Conway, J. F., Gronenborn, A. M., and Wetzel, R. (2009) Polyglutamine disruption of the huntingtin exon 1 N terminus triggers a complex aggregation mechanism. *Nat. Struct. Mol. Biol.* **16,** 380–389

25. Stadtman, E. R. (1990) Metal ion-catalyzed oxidation of proteins. Biochemical mechanism and biological consequences. *Free Radic Biol. Med.* **9,** 315–325
26. Díaz-Hernández, M., Moreno-Herrero, F., Gómez-Ramos, P., Morán, M. A., Ferrer, I., Baró, A. M., Avila, J., Hernández, F., and Lucas, J. J. (2004) Biochemical, ultrastructural, and reversibility studies on huntingtin filaments isolated from mouse and human brain. *J. Neurosci.* **24,** 9361–9371
27. Beal, M. F., and Ferrante, R. J. (2004) Experimental therapeutics in transgenic mouse models of Huntington's disease. *Nat. Rev. Neurosci.* **5,** 373–384
28. Gu, X., Greiner, E. R., Mishra, R., Kodali, R., Osmand, A., Finkbeiner, S., Steffan, J. S., Thompson, L. M., Wetzel, R., and Yang, X. W. (2009) Serines 13 and 16 are critical determinants of full-length human mutant huntingtin induced disease pathogenesis in HD mice. *Neuron* **64,** 828–840
29. Steffan, J. S., Agrawal, N., Pallos, J., Rockabrand, E., Trotman, L. C., Slepko, N., Illes, K., Lukacsovich, T., Zhu, Y. Z., Cattaneo, E., Pandolfi, P. P., Thompson, L. M., and Marsh, J. L. (2004) SUMO modification of Huntingtin and Huntington's disease pathology. *Science* **304,** 100–104
30. Vogt, W. (1995) Oxidation of methionyl residues in proteins. Tools, targets, and reversal. *Free Radic Biol. Med.* **18,** 93–105
31. Dong, J., Atwood, C. S., Anderson, V. E., Siedlak, S. L., Smith, M. A., Perry, G., and Carey, P. R. (2003) Metal binding and oxidation of amyloid-beta within isolated senile plaque cores. Raman microscopic evidence. *Biochemistry* **42,** 2768–2773
32. Canello, T., Engelstein, R., Moshel, O., Xanthopoulos, K., Juanes, M. E., Langeveld, J., Sklaviadis, T., Gasset, M., and Gabizon, R. (2008) Methionine sulfoxides on PrPSc. A prion-specific covalent signature. *Biochemistry* **47,** 8866–8873
33. Glaser, C. B., Yamin, G., Uversky, V. N., and Fink, A. L. (2005) Methionine oxidation, alpha-synuclein and Parkinson's disease. *Biochim. Biophys. Acta* **1703,** 157–169
34. Wolschner, C., Giese, A., Kretzschmar, H. A., Huber, R., Moroder, L., and Budisa, N. (2009) Design of anti- and pro-aggregation variants to assess the effects of methionine oxidation in human prion protein. *Proc. Natl. Acad. Sci. U.S.A.* **106,** 7756–7761
35. Wong, Y. Q., Binger, K. J., Howlett, G. J., and Griffin, M. D. (2010) Methionine oxidation induces amyloid fibril formation by full-length apolipoprotein A-I. *Proc. Natl. Acad. Sci. U.S.A.* **107,** 1977–1982
36. Sawaya, M. R., Sambashivan, S., Nelson, R., Ivanova, M. I., Sievers, S. A., Apostol, M. I., Thompson, M. J., Balbirnie, M., Wiltzius, J. J., McFarlane, H. T., Madsen, A. Ø., Riekel, C., and Eisenberg, D. (2007) Atomic structures of amyloid cross-beta spines reveal varied steric zippers. *Nature* **447,** 453–457
37. Kim, M. W., Chelliah, Y., Kim, S. W., Otwinowski, Z., and Bezprozvanny, I. (2009) Secondary structure of Huntingtin amino-terminal region. *Structure* **17,** 1205–1212
38. Williamson, T. E., Vitalis, A., Crick, S. L., and Pappu, R. V. (2010) Modulation of polyglutamine conformations and dimer formation by the N-terminus of huntingtin. *J. Mol. Biol.* **396,** 1295–1309
39. Lakhani, V. V., Ding, F., and Dokholyan, N. V. (2010) Polyglutamine induced misfolding of huntingtin exon1 is modulated by the flanking sequences. *PLoS Comput. Biol.* **6,** e1000772
40. Sivanandam, V. N., Jayaraman, M., Hoop, C. L., Kodali, R., Wetzel, R., and van der Wel, P. C. (2011) The aggregation-enhancing huntingtin N-terminus is helical in amyloid fibrils. *J. Am. Chem. Soc.* **133,** 4558–4566
41. Gellman, S. H. (1991) On the role of methionine residues in the sequence-independent recognition of nonpolar protein surfaces. *Biochemistry* **30,** 6633–6636
42. Arrasate, M., Mitra, S., Schweitzer, E. S., Segal, M. R., and Finkbeiner, S. (2004) Inclusion body formation reduces levels of mutant huntingtin and the risk of neuronal death. *Nature* **431,** 805–810
43. Nekooki-Machida, Y., Kurosawa, M., Nukina, N., Ito, K., Oda, T., and Tanaka, M. (2009) Distinct conformations of in vitro and in vivo amyloids of huntingtin-exon1 show different cytotoxicity. *Proc. Natl. Acad. Sci. U.S.A.* **106,** 9679–9684
44. Stack, E. C., Kubilus, J. K., Smith, K., Cormier, K., Del Signore, S. J., Guelin, E., Ryu, H., Hersch, S. M., and Ferrante, R. J. (2005) Chronology of behavioral symptoms and neuropathological sequela in R6/2 Huntington's disease transgenic mice. *J. Comp. Neurol.* **490,** 354–370
45. Weiss, A., Klein, C., Woodman, B., Sathasivam, K., Bibel, M., Régulier, E., Bates, G. P., and Paganetti, P. (2008) Sensitive biochemical aggregate detection reveals aggregation onset before symptom development in cellular and murine models of Huntington's disease. *J. Neurochem.* **104,** 846–858
46. Gutekunst, C. A., Li, S. H., Yi, H., Mulroy, J. S., Kuemmerle, S., Jones, R., Rye, D., Ferrante, R. J., Hersch, S. M., and Li, X. J. (1999) Nuclear and neuropil aggregates in Huntington's disease. Relationship to neuropathology. *J. Neurosci.* **19,** 2522–2534
47. Ding, F., Furukawa, Y., Nukina, N., and Dokholyan, N. V. (2012) Local unfolding of Cu,Zn superoxide dismutase monomer determines the morphology of fibrillar aggregates. *J. Mol. Biol.* **421,** 548–560
48. Laidman, J., Forse, G. J., and Yeates, T. O. (2006) Conformational change and assembly through edge beta strands in transthyretin and other amyloid proteins. *Acc. Chem. Res.* **39,** 576–583
49. Liu, C., Sawaya, M. R., and Eisenberg, D. (2011) β-microglobulin forms three-dimensional domain-swapped amyloid fibrils with disulfide linkages. *Nat. Struct. Mol. Biol.* **18,** 49–55
50. Angers, R. C., Kang, H. E., Napier, D., Browning, S., Seward, T., Mathiason, C., Balachandran, A., McKenzie, D., Castilla, J., Soto, C., Jewell, J., Graham, C., Hoover, E. A., and Telling, G. C. (2010) Prion strain mutation determined by prion protein conformational compatibility and primary structure. *Science* **328,** 1154–1158
51. Tanaka, M., Chien, P., Naber, N., Cooke, R., and Weissman, J. S. (2004) Conformational variations in an infectious protein determine prion strain differences. *Nature* **428,** 323–328